Journal of Energy Storage 79 (2024) 110061

Contents lists available at ScienceDirect

Journal of Energy Storage

journal homepage: www.elsevier.com/locate/est

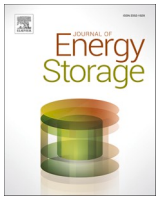

Research papers

Design improvement of latent heat thermal energy storage in wavy channel enclosures using neural networks

Hakim S. Sultan [a], Mohammed Hasan Ali [b], Jana Shafi [c], Mehdi Fteiti [d], Manuel Baro [e], Khalid Almutairi [f], Mohammad S. Islam [g], Kamal Harb [h], Fawaz S. Alharbi [i], Mohammad Ghalambaz [j,*]

[a] College of Engineering, University of Warith Al-Anbiyaa, Karbala 56001, Iraq
[b] Computer Techniques Engineering Department, Faculty of Information Technology, Imam Ja'afar Al-Sadiq University, Baghdad 10021, Iraq
[c] Department of Computer engineering and information, College of Engineering in Wadi Alddawasir, Prince Sattam bin Abdulaziz University, Saudi Arabia
[d] Physics Department, Faculty of Science, Umm Al-Qura University, Makkah 24381, Saudi Arabia
[e] Tecnológico Nacional de México Campus Nuevo Casas Grandes, Nuevo Casas Grandes, Chih., Mexico
[f] Applied College, Mechanical Engineering Technology, University of Hafr Al Batin, Hafr Al Batin, Saudi Arabia
[g] School of Mechanical and Mechatronic Engineering, Faculty of Engineering and Information Technology, University of Technology Sydney, Ultimo, NSW 2007, Australia
[h] Electrical Engineering, University of Hafr Al Batin, Hafr Al Batin, Saudi Arabia
[i] Department of Mechanical Engineering, College of Engineering, University of Hafr Al Batin, P.O. Box 1803, Hafr Al Batin 39524, Saudi Arabia
[j] Laboratory on Convective Heat and Mass Transfer, Tomsk State University, Tomsk, Russia

ARTICLE INFO

Keywords:
Wavy wall enclosure
Anisotropic metal foams
Latent heat thermal energy storage
Neural networks aided design
Phase change materials

ABSTRACT

This study conducts an in-depth analysis of latent heat thermal energy storage (LHTES) in a uniquely designed wavy enclosure filled with anisotropic copper metal foam saturated by paraffin wax. It is subjected to a high-temperature fluid stream on its top and bottom wavy walls, with its side walls well-insulated. The enclosure serves as a test bed to scrutinize the melting dynamics of paraffin wax as a Phase Change Material (PCM). The primary relations for conservation of mass, momentum, and energy were written as partial differential equations and solved using the finite element method. Among the novel aspects of this work is the exploration of wavy wall topographies defined by wave amplitude and wave number. The investigation reveals that an increase in wave amplitude generally boosts key parameters like melt volume fraction, stored thermal energy, and average temperature in the LHTES system, albeit at the slight expense of reduced heat flux at the top wavy wall. Furthermore, the study investigates the impact of anisotropic angles in the copper foam and uncovers that a 90° anisotropic angle remarkably elevates all performance indicators without requiring additional material or weight. Increasing the anisotropic angle from 0° to 90° reduces the melting duration from 3750 s to 2500 s, representing a 33 % decrease in melting time. Leveraging high-accuracy neural network (NN) models, the research also offers insights into the system's response to variations in control variables like wave amplitude, wave number, and porosity. This approach significantly reduces computational time, allowing for a comprehensive analysis of many design configurations that would otherwise be computationally prohibitive.

1. Introduction

The ever-increasing demand for sustainable and efficient energy systems has elevated the significance of thermal energy storage (TES) as a pivotal technology in fields ranging from renewable energy harvesting [1] to industrial waste heat recovery [2]. Among various TES methods, Latent Heat Thermal Energy Storage (LHTES) units, which exploit phase change materials (PCMs), have been lauded for their relatively stable operating temperature and compact energy storage. However, the effectiveness of LHTES systems is often constrained by challenges such

* Corresponding author.
E-mail addresses: hakim.s@uowa.edu.iq (H.S. Sultan), mohammed.hasan@sadiq.edu.iq (M.H. Ali), j.jana@psau.edu.sa (J. Shafi), mafteiti@uqu.edu.sa (M. Fteiti), mbaro@itsncg.edu.mx (M. Baro), khalid.almutairi@uhb.edu.sa (K. Almutairi), mohammadsaidul.islam@uts.edu.au (M.S. Islam), kharb@uhb.edu.sa (K. Harb), dr.fawaz.s.h@uhb.edu.sa (F.S. Alharbi), m.ghalambaz@gmail.com (M. Ghalambaz).

https://doi.org/10.1016/j.est.2023.110061
Received 25 October 2023; Received in revised form 30 November 2023; Accepted 7 December 2023

as poor thermal conductivity of PCMs and suboptimal heat transfer mechanisms [3], limiting their real-world applications.

In this complex landscape, optimizing the design of LHTES units has become a pressing concern. While robust, traditional analytical and numerical methods often require simplifications that might not adequately capture the intricate phenomena involved in phase-change processes. Moreover, these techniques can be computationally intensive and may not be feasible for design optimization involving multiple variables and constraints. This is where machine learning techniques, particularly neural networks, offer a transformative potential [4,5]. Neural networks can model complex, nonlinear relationships efficiently, and their ability to learn from data makes them a suitable tool for predicting and optimizing LHTES performance. Another frontier of innovation is in the enclosure's design, which houses the PCM. Wavy channel enclosures have shown promise in enhancing heat transfer rates by increasing surface area and disrupting fluid flow, thus promoting higher convective heat transfer coefficients. Combining the computational capabilities of neural networks with thermally efficient designs like wavy channel enclosures could usher in a new era of LHTES systems that are not only efficient but also optimized for a variety of applications.

Convection heat transfer within wavy enclosures, often referred to as cavities, has garnered significant consideration due to its applicability in a wide range of industrial processes and renewable energy systems. These wavy configurations are particularly interesting because they disrupt the laminar flow and increase heat transfer surface area, thus encouraging enhanced heat transfer mechanisms [6,7]. Among the various modes of heat transfer, natural convection stands out for its passive feature, requiring no external work for the transfer of energy. Studies utilizing hybrid nanofluids such as water–Cu–Al_2O_3 have revealed that natural convection in wavy enclosures can lead to higher Nusselt numbers when compared to pure fluids and other regular nanofluids. These nanofluids offer thermal advantages by improving heat transfer percentages by 5–13.7 % [6]. Investigations into mixed convection in rectangular wavy enclosures with multiple solid fins found that high-concentration nanofluids alone could boost the rate of heat transfer even without applying magnetic fields. The optimal heat mechanisms were found to occur under natural convection conditions with high Richardson numbers [7]. The geometry and physical conditions of the wavy enclosure also critically impact the convection heat transfer. Research on porous cavities filled with hybrid nanofluids showed that parameters like the Darcy number, Rayleigh number, and amplitude of the wavy wall considerably impact convection flow [8]. For instance, conduction becomes the dominant heat transfer mechanism at high Darcy numbers, overshadowing convection [9]. Similar insights were found in studies investigating the effect of aspect ratios and a partial heat source in wavy porous cavities [10].

Different modeling approaches, like the Galerkin finite element method, have provided accurate heat transfer predictions in these complex geometries [6,9,11]. These numerical methods have been instrumental in understanding the impacts of such factors as inclination angles and number of undulations on heat transfer rates [8,11,12].

The literature review shows diverse finned structures characterized by low thermal conductivity aimed at improving the efficiency of PCMs. Significantly enhanced performance, up to 86.3 %, is observed in cylindrical LHTES units utilizing topology-optimized fin designs derived through radial and axial optimization. Paraffin RT35 serves as the PCM, and water is the heat transfer fluid in these units [13]. Radially finned structures are particularly effective for large-scale applications, which occupy 20 % of the initial PCM volume. In the context of a rectangular enclosure, research focuses on the impact of corrugated fins on the solid-liquid phase transformation of PCM [14]. The study reveals that longer and thicker fins contribute to improved melting rates, average temperatures, and thermal energy storage capacities. Corrugated fins, inducing increased flow perturbations, further enhance melting performance. Through a data-driven approach, an optimized corrugated fin geometry demonstrates a 43 % increase in thermal energy storage per unit mass compared to planar fins [14]. A distinctive tree-pin-shaped fin is introduced in a laboratory-scale shell-and-tube latent thermal energy storage unit employing adipic acid as PCM [15]. In comparison to traditional longitudinal fins, these tree-pin-shaped fins significantly accelerate charging and discharging speeds, reducing charging time by 44.6 % and discharge time by 50.6 %. Notably, these fins do not impede natural convection at any orientation, indicating potential application versatility [15].

The increasing demand for efficient TES systems has drawn significant attention to integrating PCMs with high-conductive matrices like metal foams. These hybrid systems are designed to optimize both the heat transfer rate and the total stored energy, thereby addressing the dual constraints of performance and storage capacity. Due to their high thermal conductivity, metal foams are an excellent medium for enhancing the heat transfer rate in PCMs [16,17]. Their porous structure facilitates the convective melting of PCMs, resulting in accelerated phase transitions and more efficient energy storage. The properties of metal foam, such as porosity and pore density, are also affected by the thermal performance. A study found that low-porosity metal foam could significantly reduce temperature variation due to increased thermal conductivity. However, higher heat fluxes led to local temperature differentiations that could exceed 50 °C depending on pore density [16]. The spatial arrangement of metal foam within the storage system is another optimization parameter. Research indicates that inserting the foam layer diagonally from corner to corner led to minimal melting time. The optimum porosity was 88 %, allowing almost the same stored energy as pure PCM [17].

The pore-level study on PCMs integrated into metal foam architectures featuring the Kelvin cells highlighted that such configurations significantly increased the overall heat transfer rate and reduced melting time [18]. This adds another dimension to our understanding by suggesting that the pore-scale structure could be critical in influencing melting dynamics and storage capacity. Random porosity distribution, rather than uniform, has also been investigated. The former might provide up to a 10 % lower rate of PCMs melting for a similar average porosity [19]. Additionally, using anisotropic metal foams could offer significant gains in thermal energy storage power, potentially saving up to 20 % in charging time without affecting the unit's weight or storage capacity [20]. In practical applications, like domestic air heaters, using PCM-metal foam composites effectively provides a uniform output temperature, which is crucial for efficient space heating [21].

The shape of the enclosure or cavity that houses phase change materials (PCMs) in heat transfer applications is critical for optimizing the system's performance. Various studies have experimented with different geometries, including annuli, wavy tubes, trapezoidal enclosures, and more, to understand their impact on heat transfer efficiency and thermal energy storage rate. An annular enclosure is commonly used for confining PCMs in applications that deal with conjugate solid-liquid phase change heat transfer. This geometry effectively caters to pulse heat loads by enhancing heat transfer at the hot surface, especially when the annuli are filled with a composite of PCM and metal foam [22]. The shape allows the enthalpy-porosity approach and Darcy-Brinkman model to be effectively utilized, yielding promising results, particularly at low external cooling power. Another intriguing geometry involves using wavy tubes filled with nano-enhanced PCM and metal foams. The tubes' wavy nature was studied to understand their effect on thermal response time, stored energy, and heat transfer behavior. Interestingly, while adding complexity to the design, like wavy tubes, may offer some advantages, a simple tube structure with no wavy surface resulted in better charging power [23]. Trapezoidal cavities have also been researched, particularly focusing on the orientation of the cavity and the impact of nanoparticle additives on the PCM. For instance, embedding the PCM in a trapezoidal cavity filled with paraffin wax showed that orientation could significantly affect the performance [24]. Another study with a trapezoidal geometry utilized fin extensions to improve thermal conductivity, thereby reducing the melting time [25].

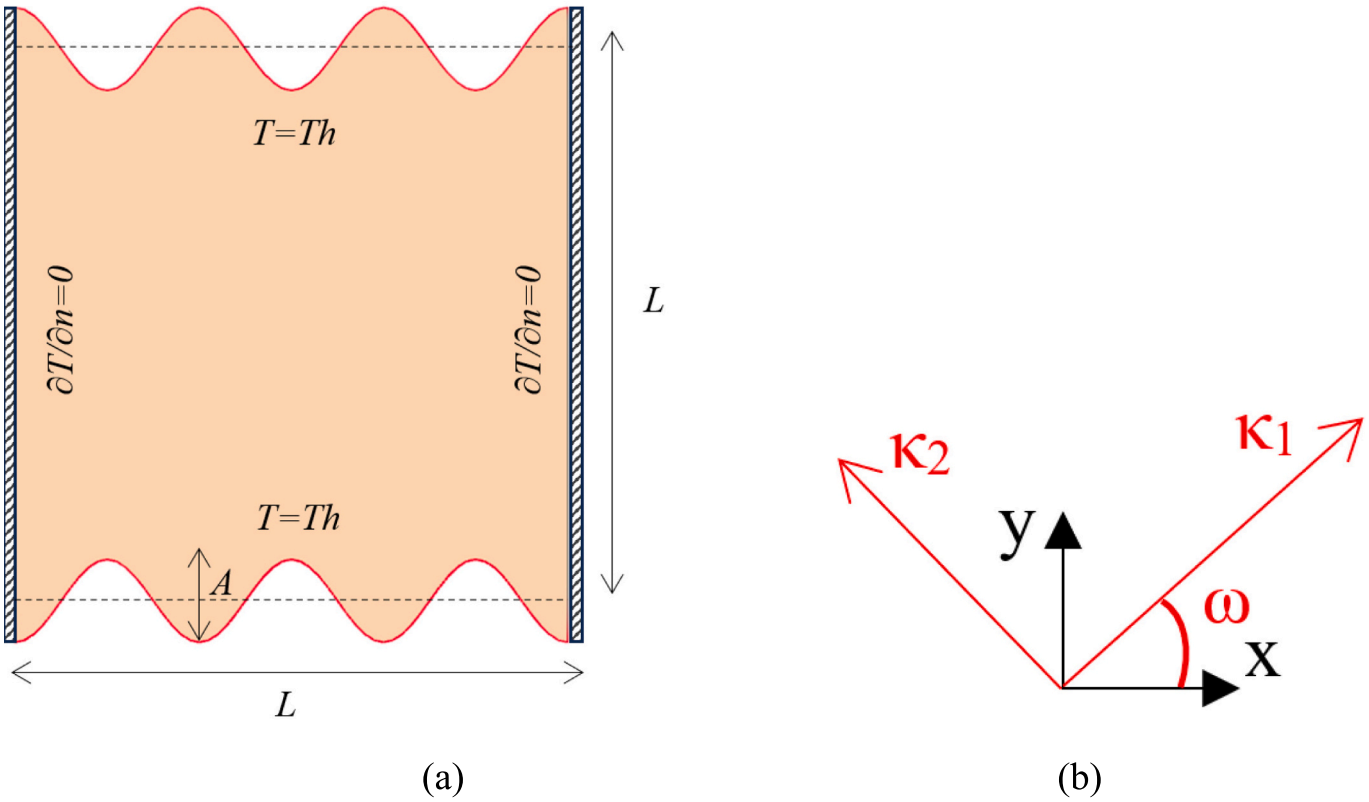

Fig. 1. Diagram depicting the 2D model of the wavy enclosure featuring an anisotropic MF saturated by paraffin wax. (a) Detailed view of the enclosure; (b) Explanation of anisotropic angle orientations.

The shape of additional elements within the enclosure, such as metal foams, also plays a crucial role. For instance, studies have shown that forming metal foam layers could impact the thermal energy storage power by up to 60 % [26]. Other techniques, like using internal and external fins in an annular enclosure, have been studied to enhance the melting rate of the PCM, reducing melting time by over 60 % when optimized [26]. In applications like air-conditioning systems, it has been observed that even the inlet velocity and PCM volume can affect the shape and performance of the cavity. Higher inlet velocities lead to shorter melting durations, thereby affecting the overall performance [27].

ANNs have increasingly become essential tools in heat transfer, particularly in predicting the behavior of PCMs, nanofluids, and thermal systems. ANNs offer a robust computational methodology to model complex relationships between variables, thereby facilitating more accurate predictions and enabling more effective thermal management solutions. In the domain of transient heat transfer, ANNs have been used to model the characteristics of a PCM heat sink. A feedforward back-propagation multilayer perceptron (MLP) was employed to predict the transient heat transfer in a PCM heat sink under differing power conditions. The ANN model demonstrated high accuracy in predicting the Nusselt number during the melting of the PCM. The study confirmed that using PCMs in heat sinks effectively reduces transient temperature, providing valuable insights into the thermal management of electronics [28].

ANNs are also applied to study the heat transfer properties of nanofluids in channels. By considering various parameters like nanoparticle concentration, expansion ratio, and Reynolds number, neural networks help to estimate the heat transfer rate more reliably than traditional methods [29]. Further, ANNs have proven exceptionally accurate in predicting the thermal conductivity of nanofluids. For instance, using ANNs trained with the Levenberg–Marquardt algorithm has yielded models with high confidence levels ($R_2 = 0.9987$) when compared to other methods like MARS ($R_2 = 0.9879$) or GMDH ($R_2 = 0.9980$) [30]. In another study focusing on nanofluids containing CuO nanoparticles, ANNs outperformed polynomial models with remarkably lower average absolute relative deviation values, thereby making them a more reliable choice for predicting thermal conductivity [31].

The literature review shows phase change heat transfer and energy storage in LHTES units is an important topic in renewable energy and waste heat recovery. The shape of PCM enclosures and metal foams can significantly impact the heat transfer rate and the efficiency of LHTES units. The heat transfer in wavy wall enclosures has been the subject of several recent studies [6–12]. A wavy wall delivers an extended heat transfer surface and can also disrupt the fluid flow and enhance heat transfer. Thus, the present study aims to address the phase change heat transfer of PCMs in a wavy wall LHTES unit for the first time. An ANN further analyzes the heat transfer behavior of the LHTES for design parameters.

2. Model description

A wavy enclosure is filled by an anisotropic copper metal foam saturated by paraffin wax. The top and bottom wavy walls are subject to a hot fluid stream at a high temperature *Th*, while the left and right borders are well insulated. A schematic view of the enclosure is illustrated in Fig. 1(a). The wavy shape of the top and bottom walls provides an extended surface area for heat transfer. The wavy surfaces can also provide effective structural mechanical stability. The paraffin is initially at a super cold temperature *Tc*. The wavy surface is introduced using a wave amplitude (A) and a wave number (σ) as:

$$y = A\sin(2\pi\sigma x - \pi/2) \text{ on bottom} \tag{1a}$$

$$y = L + \mathrm{A}\ \sin(2\pi\sigma x + \pi/2) \text{ on the top} \tag{1b}$$

Table 1
An overview of the thermophysical properties of the materials under consideration.

Materials	C_p (J/kg.K)	ρ (kg/m^3)	k (W/m.K)	l (kJ/kg)	T_m (°C)	β (1/K)	μ (kg/m.s)
Copper foam [47]	386	8900	380	–	–	–	–
Paraffin (solid/liquid) [48–50]	2700/2900	916/790	0.21/0.12	176	49–54	0.00091	0.0036

Paraffin was embedded in copper metal foam (MF) for better thermal conductivity of the composite MF-paraffin. Paraffin inside MF can melt at an average fusion temperature of $T_l \sim 51$ °C [32]. Copper foam was selected for its favorable thermal conductivity and ease of synthesis, while paraffin wax was chosen for its cost-effectiveness and suitability for temperature energy storage. Upon phase change, paraffin absorbs a significant amount of latent heat and stores the thermal energy. The temperature gradients inside the molten paraffin induce density gradients, which lead to buoyancy force and natural convection flows inside the liquid-saturated regions of the metal foam.

For a fixed amount of mass and porosity, an anisotropic MF could be engineered with thick and thin ligaments at orthogonal directions as explained in [20,33,34], resulting in improved thermal conductivity in one direction (direction of thick ligaments) and reduced thermal conductivity at the orthogonal direction. The MF permeability can be altered as well. The orthogonal directions of anisotropic MF can be placed at an arbitrary angle (ω) related to a fixed coordinate system of x and y, as illustrated in Fig. 1(b). Besides, the enclosure size was set as L = 15 cm. The following section provides the mathematical equations pertaining to the physical behavior of the system during the energy storage (melting process) of the paraffin wax.

2.1. Governing equations

The equations that govern the heat transfer in the melting process of paraffin wax consist of those for conserving energy, mass, and momentum. To separately account for the local temperatures of both the copper MF and the paraffin wax, a dual-temperature equation was employed [23,35,36]:

Mass conservation:

$$\nabla \boldsymbol{u} = 0 \tag{2}$$

Momentum conservation:

$$\frac{\rho_{\text{Paraffin}}}{\varepsilon}\frac{\partial \mathrm{u}}{\partial t} + \frac{\rho_{\text{Paraffin}}}{\varepsilon^2}\nabla.(\mathrm{u}\otimes\mathrm{u}) = -\nabla p + \frac{\mu_{\text{Paraffin}}}{\varepsilon}\nabla.(\nabla \mathrm{u}) - \frac{\mu_{\text{Paraffin}}}{\kappa}\mathrm{u} - \rho_{\text{Paraffin}}\frac{C_F}{\sqrt{\kappa}}|\mathrm{u}|\mathrm{u} + A_{mush}\frac{(1-\phi(T))^2}{\iota+\phi^3(T)}\mathrm{u} + g\rho_{\text{Paraffin}}\beta_{\text{Paraffin}}(T-T_0)\hat{j} \tag{3}$$

Energy conservation in paraffin:

$$\varepsilon(\rho C_p)_{\text{Paraffin}}\frac{\partial T_{\text{Paraffin}}}{\partial t} + (\rho C_p)_{\text{Paraffin}}\mathrm{u}.\nabla T_{\text{Paraffin}} = \nabla.\left(k_{\text{eff,Paraffin}}\nabla T\right) + h_v\left(T_{\text{Copper}} - T_{\text{Paraffin}}\right) - \varepsilon\rho_{\text{Paraffin}}l_{\text{Paraffin}}\frac{\partial \phi(T)}{\partial t} \tag{4}$$

Energy conservation in copper MF:

$$(1-\varepsilon)(\rho C_p)_{Copper}\frac{\partial T_{\text{Copper}}}{\partial t} = \nabla.\left(k_{\text{eff,Copper}}\nabla T_{\text{Copper}}\right) - h_v\left(T_{\text{Copper}} - T_{\text{Paraffin}}\right) \tag{5}$$

In the equations under discussion, several parameters are incorporated, including the porous permeability (κ), the Forchheimer parameter (C_F), the coefficient for volume expansion due to thermal effects (β), the acceleration due to gravity (g), and the latent heat associated with fusion (l). The model also includes the volumetric form of the interstitial heat transfer coefficient (h_v), derived from the pore-scale Nusselt number, which can be computed from [37]. The abbreviations 'Copper,' 'Paraffin,' and 'eff' are indicative of copper metal foam, phase-change materials of paraffin, and effective properties, respectively. Besides, the source term parameters were put as $A_{\text{mush}} = 10^{10}$ Pa·s/m^2 and ι = 0.001. As discussed in [38–40], the permeability coefficient (A_{mush}) value can influence the solution accuracy. Here, the value of A_{mush} was adopted higher than its typical value for clear flow (10^5–10^7) since the flow velocities for free convection in porous metal foams are pretty slow, and the permeability of metal foam is small. Thus, as adopted in current research, a fairly large value of A_{mush} for metal foams is essential.

According to the information in reference [41], the influence of pore architecture on thermal conductivities has been accounted for by incorporating the effective thermal conductivities for both copper ($k_{\text{eff, Copper}}$) and paraffin ($k_{\text{eff, Paraffin}}$). Further information on effective thermal conductivities can be found in [35,41]. In reference [42], further clarification is provided regarding the melting volume fraction influenced by temperature, denoted as ϕ:

$$\phi(T) = \begin{cases} 0 & T < T_l - \frac{1}{2}\Delta T_l \text{ (Solid phase)} \\ \frac{1}{2} + \frac{(T-T)}{\Delta T_l}T_l - \frac{1}{2}\Delta T_l \le T \le T_l + \frac{1}{2}\Delta T_l & \text{(Liquid-Solid mushy region)} \\ 1 & T > T_l + \frac{1}{2}\Delta T_l \text{ (Liquid phase)} \end{cases} \tag{6}$$

where eight degrees was selected for the phase change temperature range. In an anisotropic metal foam (AMF), both thermal conductivity and permeability exhibit directional variations introduced as [43]:

$$k_{\text{eff,MF}} = \begin{bmatrix} k_2(sin\omega)^2 + k_1(cos\omega)^2 & (k_1-k_2)(cos\omega)(sin\omega) \\ (k_1-k_2)(cos\omega)(sin\omega) & k_1(sin\omega)^2 + k_2(cos\omega)^2 \end{bmatrix} \tag{7}$$

$$\kappa = \begin{bmatrix} \kappa_2(sin\omega)^2 + \kappa_1(cos\omega)^2 & (\kappa_1-\kappa_2)(sin\omega)(cos\omega) \\ (\kappa_1-\kappa_2)(sin\omega)(cos\omega) & \kappa_2(cos\omega)^2 + \kappa_1(sin\omega)^2 \end{bmatrix} \tag{8}$$

In terms of thermal conductivity and permeability for copper metal foam, k_1 and k_2 are calculated as $k_1 = (1+\Omega)\times k_{\text{m}}$ and $k_2 = (1-\Omega)\times k_{\text{m}}$, respectively. Similarly, for permeability, $\kappa_1 = (1-\Omega)\times\kappa_m$ and $\kappa_2 = (1+\Omega)\times\kappa_{\text{m}}$. Here, k_{m} and κ_m signify the average values for thermal conductivity and permeability in copper MF, which can be computed using [35,41,44], while Ω represents the factor for anisotropy. Besides, a linear weight average was adopted to calculate the thermophysical properties in the mushy region. The thermophysical properties of paraffin wax and copper foam were adopted from [32,45,46]. Table 1 provides the thermophysical properties of paraffin and copper foam.

The enclosure is initially at $T_0 = T_{\text{f}} - 15$ °C (36 °C), and the wavy walls are at $T_l = T_{\text{f}} + 15$ °C (66 °C). The vertical walls are also insulated with zero heat flux. The zero velocity was also applied on all surfaces.

The melting volume fraction denotes the average quantity of PCM that has melted and is computed using a specified equation:

$$MVF = \frac{\oint_V \varepsilon\phi dV}{\oint_V \varepsilon dV} \tag{9}$$

where dV refers to the elemental volume of the shell domain. The total thermal energy storage is obtained by adding up both latent heat and sensible heat:

Table 2
Examined meshes with various mesh parameters *Nm* and the corresponding computational time for each case.

Nm	Quads	Edge elements	Computational time (hours)
2	7200	360	2.36
3	16,471	540	6.55
4	29,161	720	12.21
5	45,451	900	18.18
6	64,800	1080	12.77

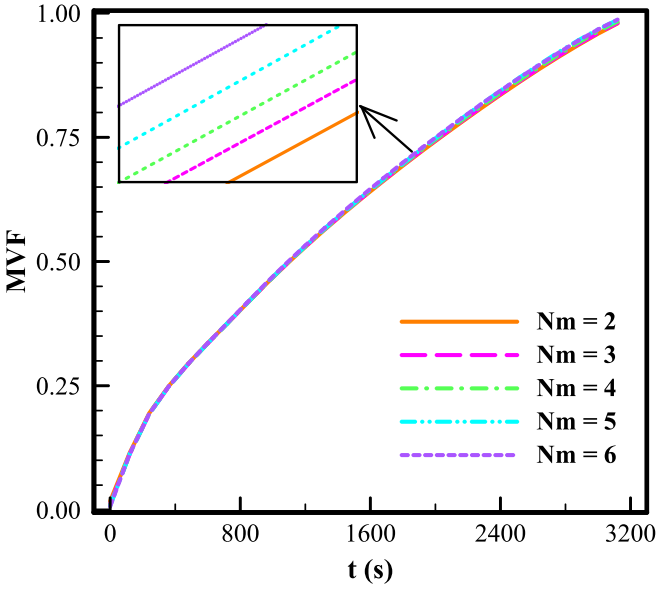

Fig. 2. The impact of mesh resolution parameter (*Nm*) on the melting and solidification process.

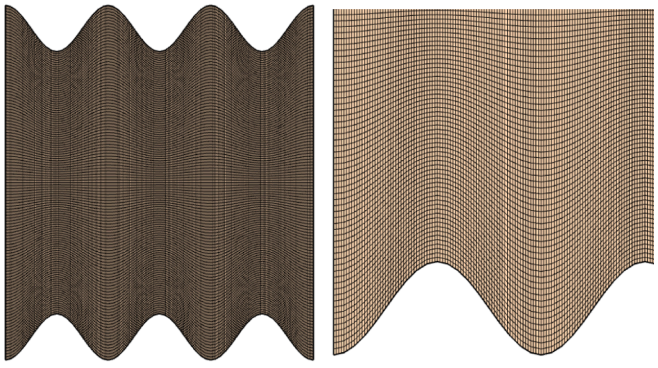

Fig. 3. A mesh view with $Nm = 4$ for (a) the entire geometry and (b) a zoomed view at the bottom left.

$$Q_t = \left[\oint_V \left(\int_{T_0}^{T} \varepsilon(\rho C_P)_{\text{Paraffin}}(T)dT_{\text{Paraffin}}\right)dV\right] + (T - T_0)(\rho C_P)_{\text{Coper}}\oint_V (1-\varepsilon)dV + \varepsilon\oint_V \rho_{\text{Paraffin}}\phi l_{\text{Paraffin}}dV \quad (10)$$

Local heat transfer rates at the top and bottom heated walls are obtained as:

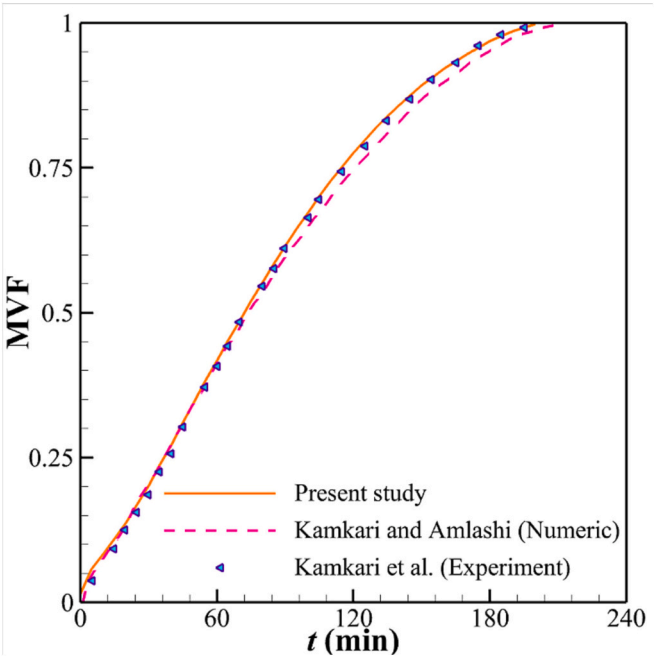

Fig. 4. Comparison between energy storage data from our present simulation and the measured values reported in the melting study from references [55,56].

$$q''_{top} = \varepsilon k_{\text{eff,Paraffin}}\left.\frac{\partial T_{\text{Paraffin}}}{\partial n}\right|_{top} + (1-\varepsilon)k_{\text{eff,Copper}}\left.\frac{\partial T_{\text{Copper}}}{\partial n}\right|_{top}$$
$$q''_{bottom} = \varepsilon k_{\text{eff,Paraffin}}\left.\frac{\partial T_{\text{Paraffin}}}{\partial n}\right|_{bottom} + (1-\varepsilon)k_{\text{eff,Copper}}\left.\frac{\partial T_{\text{Copper}}}{\partial n}\right|_{bottom} \quad (11)$$

where *n* is the wall normal vector, and the average heat transfer rate is obtained as:

$$q''_{avg,top} = \frac{\int_s q''_{top}ds}{\int_s ds},\quad q''_{avg,bottom} = \frac{\int_s q''_{bottom}ds}{\int_s ds} \quad (12)$$

where *s* is the heated wall length. The average temperature was also obtained as:

$$\Delta T_{avg} = \frac{\oint_V (T - T_0)dV}{\oint_V dV} \quad (13)$$

3. Solution method and model verification

3.1. Finite element method (FEM)

Fundamental equations, along with their boundary and initial conditions, were solved by leveraging FEM. The method effectively handled the nonlinear variables related to phase transitions [41,42]. Utilizing the weak formulation of the governing equations and opting for a second-order discretization for thermal and momentum equations, a series of residual algebraic equations were generated *via* Gauss quadrature integration on an element-by-element basis. These sets of equations underwent iterative solutions using the Newton method [51,52], with a damping coefficient of 0.9 to expedite convergence. The PARDISO parallel computational solver, working alongside the Newton method, facilitated the performance of calculations across multiple CPU cores in parallel [53,54]. Automatic adjustments were made in the solution timing and convergence to maintain a relative solution accuracy below 10^{-4}, applying a backward differential formula of first and second order.

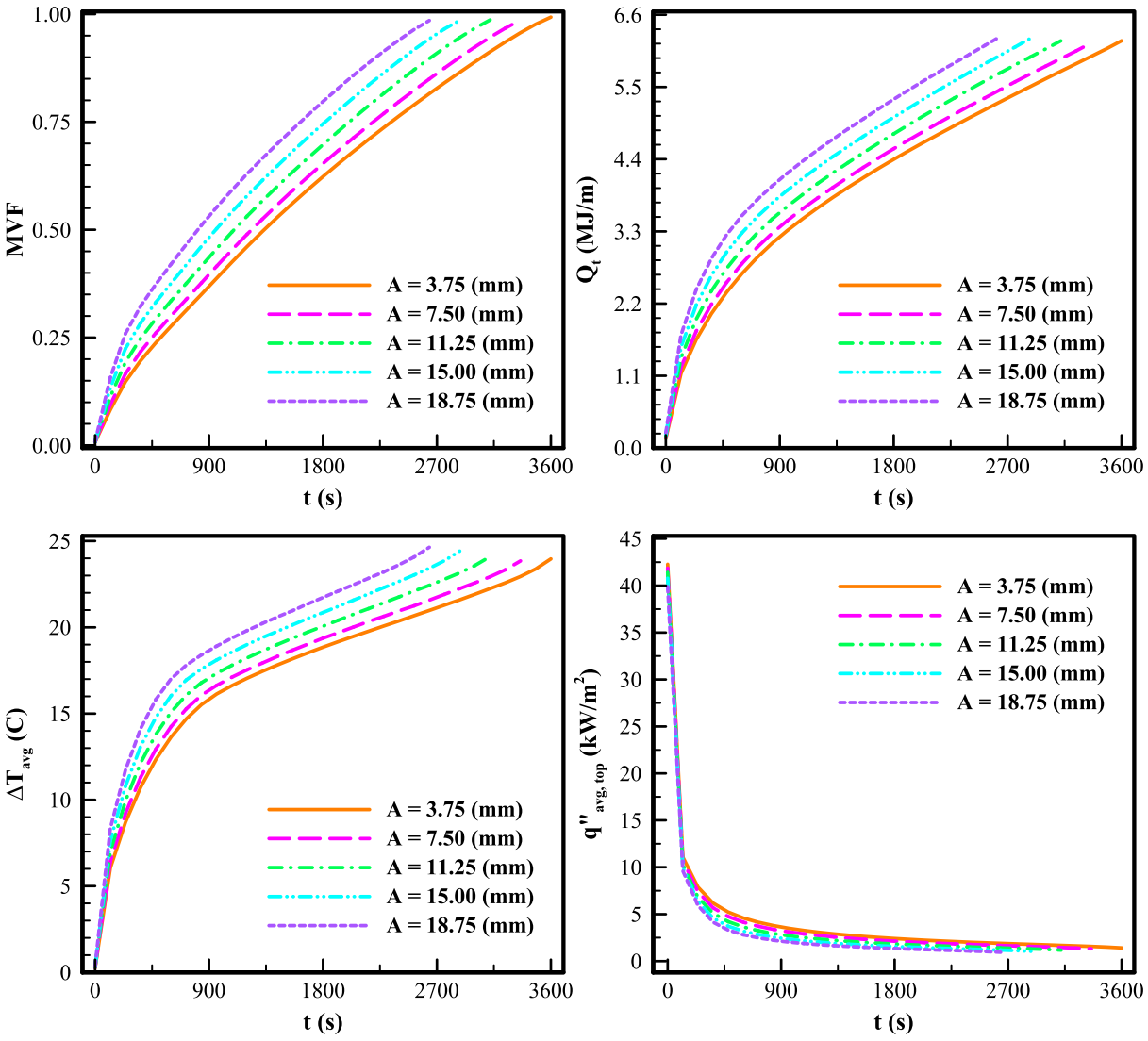

Fig. 5. MVF, total heat transfer (Q_t), average temperature difference (ΔT_{avg}), and the top wall average heat flux ($q''_{avg,\ top}$) over the melting time for different wave amplitude (A).

The advantages of FEM include high precision, uniformity, and smooth results over the discretized mesh, qualities that align well with the goals of this research. Computations began from the initial conditions and subsequently explored energy storage and phase change characteristics. The equations for thermal balance and mass continuity y, along with the phase field variable ϕ, were considered fully coupled and were solved in an iterative manner. The algorithm was designed to stop once a completely melted state was reached, as evidenced by a melting volume fraction (MVF) greater than or equal to 0.99, which served as the halting conditions.

3.2. Mesh sensitivity analysis

During the phase change of PCM, the impact of grid refinement on numerical precision was evaluated using a scenario characterized by $\Omega = 0.3$, $\omega = 45°$, $A = 1.125$ mm, $\sigma = 3$, and $\varepsilon = 0.95$.

Table 2 and Fig. 2 present a focused study on the impact of varying the mesh parameter *Nm* on computational simulations, explicitly examining the number of quadrilateral elements (Quads), edge elements, and computational time. A salient observation is the increase in mesh density, reflected by a higher number of Quads and edge elements, as *Nm* grows. While a denser mesh typically yields more accurate results, it also generally increases computational time. However, this relationship is not strictly linear. For example, the computational time for Nm = 6 is actually less than for *Nm* = 5, which is due to the backward differentiation formula (PDF) for the automatic time step. A suitably fine mesh provides a better convergence in capturing the melting interface. It leads to a reduced overall computational time by allowing the selection of larger time steps while maintaining the relative computational error low. Here, as a balance between computational cost and accuracy, the mesh control parameter *Nm* = 4 was adopted for computations. Fig. 3 shows a view of the adopted mesh.

3.3. Model verification

To evaluate the model's accuracy, we mimicked the conditions outlined by Kamkari et al. [55], focusing on phase change heat transfer coupled with natural convection (Fig. 4). The study in [55] utilized lauric acid as the PCM and conducted the melting experiments in a chamber with dimensions of 120 mm in height and 50 mm width. The chamber's left wall was maintained at an isothermal heat condition of 70 °C, starting from an initial ambient temperature of 25 °C. Lauric acid's average melting point was noted to be 46 °C. For a detailed list of lauric acid's thermophysical properties, one can consult Table 1 in [55].

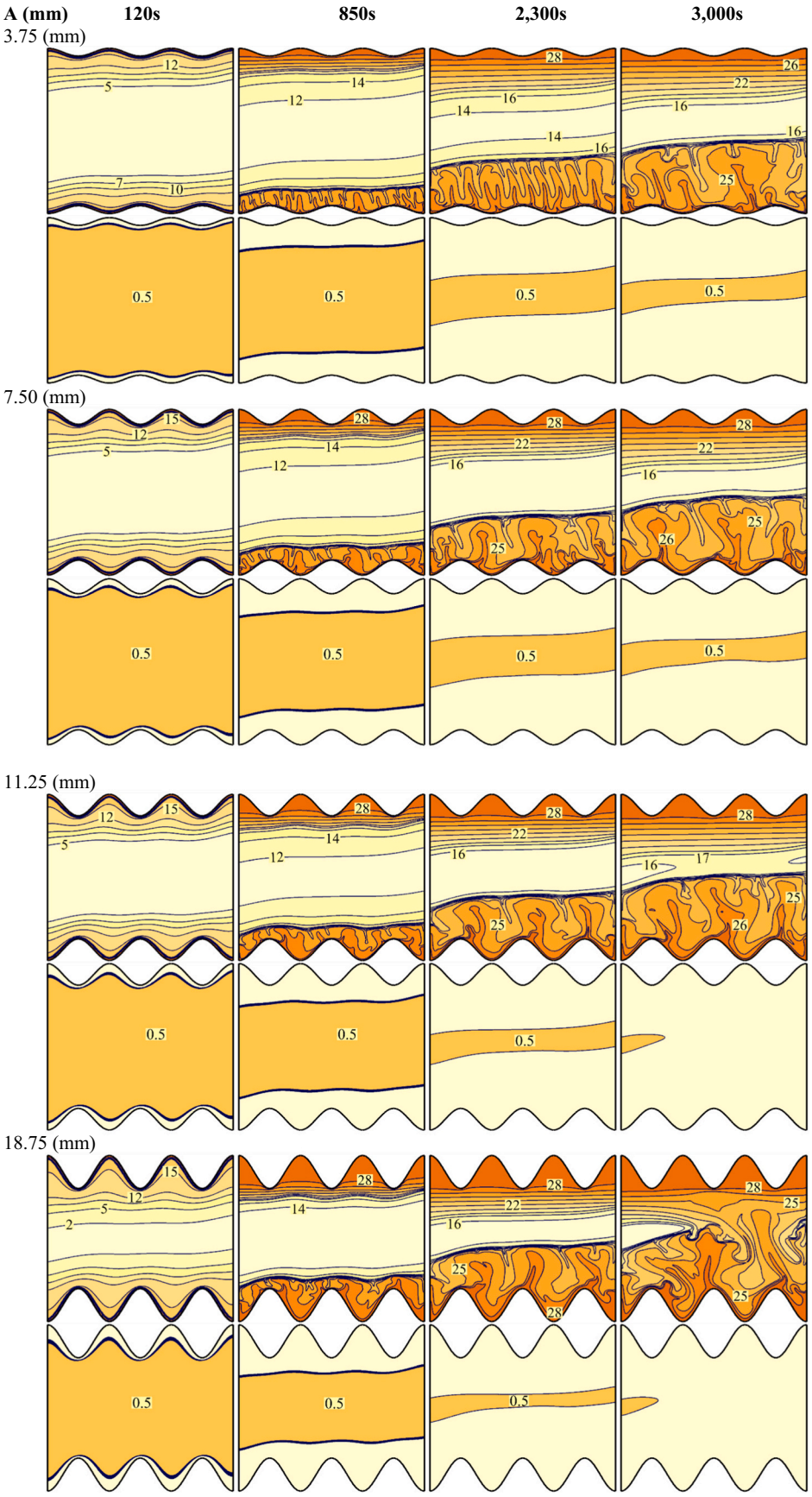

Fig. 6. Isotherms and the melting interface at selected melting time for different amplitudes *A*. The first row of each set shows the temperature difference contours (T-T_0) in °C, and the second row depicts the melting interface.

The results of the numerical study of Kamkari and Amlashi [56] have also been plotted in Fig. 6. Our model's calculated energy storage during the charging phase was closely aligned with the data presented in [43,56], as illustrated in Fig. 6.

4. Results and discussion

The anisotropic angle ($0° \leq \omega \leq 90°$), wave number $1 < \sigma < 4$, the wave amplitude 0.01125 m $< A <$ 0.01875 m, and the anisotropy factor $0 < \Omega < 0.3$ was investigated. The parameters' values used in the mesh study section serve as a reference. Unless otherwise noted, these values remain consistent; any deviations will be explicitly reported. Fig. 5 illustrates the temporal evolution of the melting volume fraction, the stored thermal energy, the average temperature difference in the LHTES unit, and the mean heat flux at the apex of the wavy wall, all as functions of varying the amplitudes of the wavy walls. It can be observed that increasing the wave amplitude enhances MVF, stored thermal energy, and average temperature within the LHTES unit. However, this inversely affects the average heat flux at the top wavy wall. The rise in MVF is explained by the enlarged surface area available for heat transfer due to larger wave amplitudes, thereby resulting in an accelerated melting rate and enhanced energy storage. This increase in stored energy consequently elevates the average temperature differential across the LHTES unit. The reduction in the average heat flux is primarily a consequence of its definitional parameter, as per Eq. (12), which averages the heat flux over the extended length of the undulating wall. As the wall length increases with greater wave amplitude, the temperature gradients become slightly less steep, thereby causing a modest decline in the average heat flux. Besides, since the model is 2D, the energy is computed per unit of length.

Fig. 6 displays the isotherms of temperature difference (T-T_0) and MVF contours for various wave amplitudes at four distinct time intervals. Henceforth, these temperature difference isotherms will be simply referred to as temperature for brevity. The figure illustrates that an increase in the wave amplitude expands the height of the wavy walls, allowing the heated surfaces to penetrate further into the solid PCM domain. Initial isotherms (t = 120 s) closely mimic the contours of the heated top and bottom wavy walls, suggesting a dominant role of pure conduction at this phase. Melting is noticeable only as a thin layer over these heated surfaces for all amplitudes A. Within the solid regions, the isotherms are primarily linear as the heat is predominantly absorbed in the melting interface, allowing only a minimal thermal gradient between the melting interface temperature (T_l) and the initial PCM temperature (T_0). As time progresses, a greater volume of PCM adjacent to the top and bottom walls undergoes phase transition. Natural convection patterns emerge within the isotherms in the molten regions at the lower part of the unit, whereas the upper sections display stratified regions without conspicuous temperature line distortions. Natural stratification occurs in the top region because the warmer melted PCM remains buoyant near the top heated wall, while the colder PCM near the melting interface stays at the bottom, thereby suppressing free convection currents in the upper region.

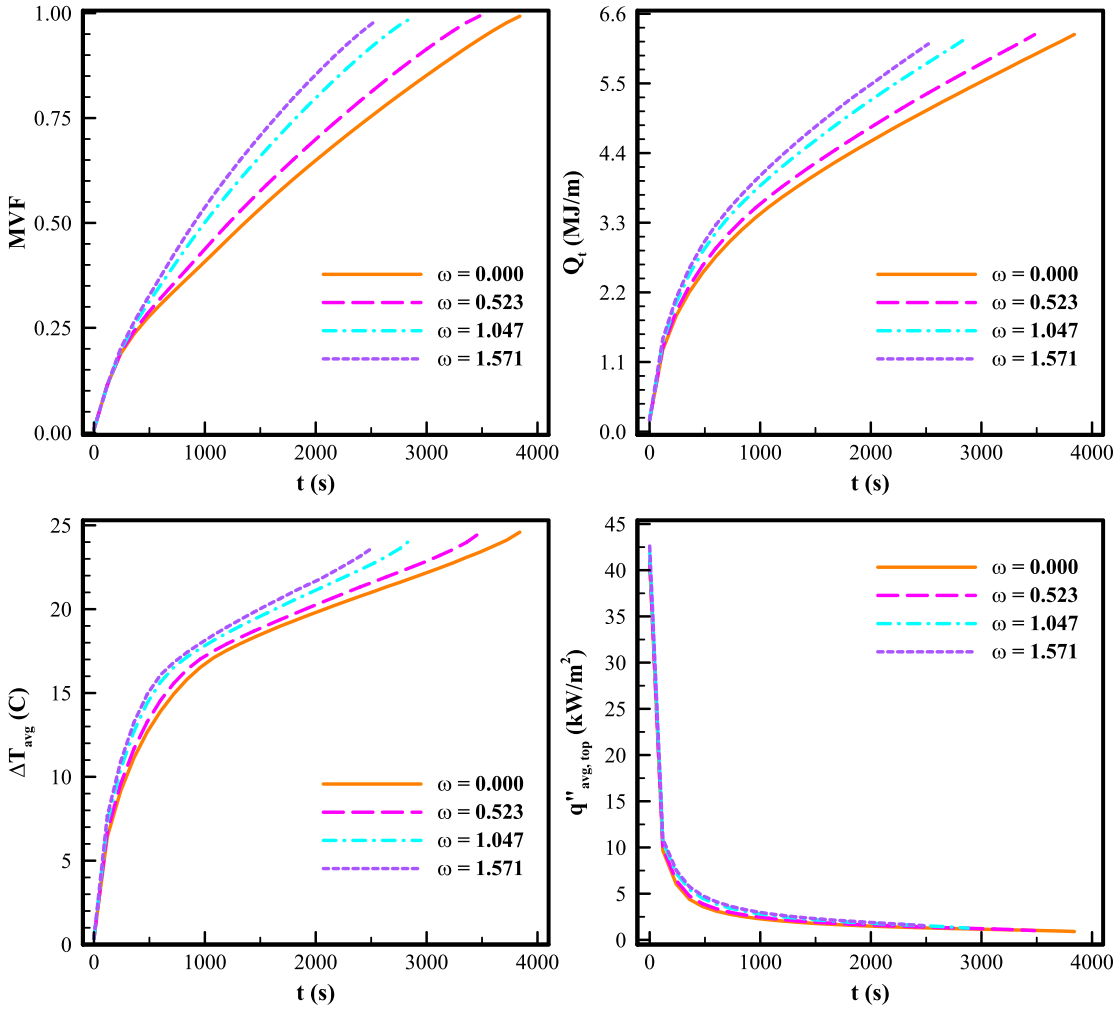

Fig. 7. MVF, total heat transfer (Q_t), average temperature difference (ΔT_{avg}), and the top wall Nusselt number over the melting time for different anisotropic angles ω (rad).

Additionally, the contours of the melting interface reveal a broader melting zone at the bottom compared to the top, which is the result of o convective heat transfer on the bottom zone. It is also evident that an increase in wave amplitude significantly expands the molten region, which is clearly noticeable at the time $t = 3000$ s. This finding corroborates the observations made in Fig. 5. An increase in wave amplitude (A) from 3.75 mm to 18.75 mm reduces the full melting time from 3600 s to 2700 s, rendering a 25 % reduction in the melting time.

Fig. 7 presents a comprehensive analysis of the LHTES unit's key performance indicators, such as melting time and energy storage rate, in relation to varying anisotropic angles (ω). A larger anisotropic angle yields significant improvements in all critical metrics. Specifically, an anisotropic angle of 1.571 rad (or 90°) results in the shortest melting time and the highest rate of energy storage. An increase of anisotropic angle from 0° to 90°, reduces the full melting time from 3750 s to 2500 s, resulting in a 33 % reduction in melting time. According to Eq. (7), this angle maximizes thermal conductivity in the y-direction, which is aligned with the primary heat transfer path between the heated wall and the solid PCM domain. Consequently, it optimizes conduction-based heat transfer. Simultaneously, high permeability in the x-direction enhances convective flow along the wavy wall, making this configuration particularly advantageous for LHTES unit design. Importantly, varying the anisotropic angle neither adds weight nor material to the system nor diminishes the unit's energy storage capacity. Enhanced thermal conductivity in the y-direction due to a higher anisotropic angle boosts the heat flux at the top wall and elevates the unit's average temperature.

Fig. 8 visualizes isotherms and melting interfaces for anisotropic angles of 0° and 90° at different stages of the melting process. Increasing the anisotropic angle (ω) broadens the molten region, especially noticeable in the upper portions where thermal conductivity in the y-direction is maximized. However, convective heat transfer is virtually non-existent because of the stratified layering of the liquid PCM in the upper regions. Therefore, the improved permeability in the x-direction does not contribute to advection mechanisms there. Conversely, the impact of a larger anisotropic angle ($\omega = 90°$) is more pronounced at the bottom region, enhancing both conduction and convection heat transfer mechanisms and thus significantly boosting the overall heat transfer efficiency.

Fig. 9 illustrates the temporal evolution of crucial parameters during the melting phase as a function of varying wave numbers (σ). Elevating the wave number enhances most key parameters but adversely impacts the average heat flux. This trend mirrors the findings in Fig. 5. The augmentation in wave number expands the surface area of the heated wall, thereby diminishing temperature gradients and consequently lowering the average heat flux. Nonetheless, it's important to emphasize that heat transfer involves a complex interplay between surface area and heat flux. Thus, the product of the expanded surface area and the heat flux can increase with a higher wave number.

Insightfully, the data plots for $\sigma = 3$ and $\sigma = 4$ demonstrate a close correlation in terms of both MVF and stored thermal energy. Therefore, elevating the wave number beyond σ = 3 offers limited advantages. As such, the LHTES unit with $\sigma = 3$ could be a preferable option, as it not only simplifies manufacturing complexities but also minimizes the consumption of wavy wall material. Concurrently, the mean temperature also ascends with the wave number, indicative of enhanced heat transfer and thermal energy storage capabilities.

Fig. 10 reveals the isotherms and contours of the melting interface at different wave numbers. A rise in wave number noticeably improves

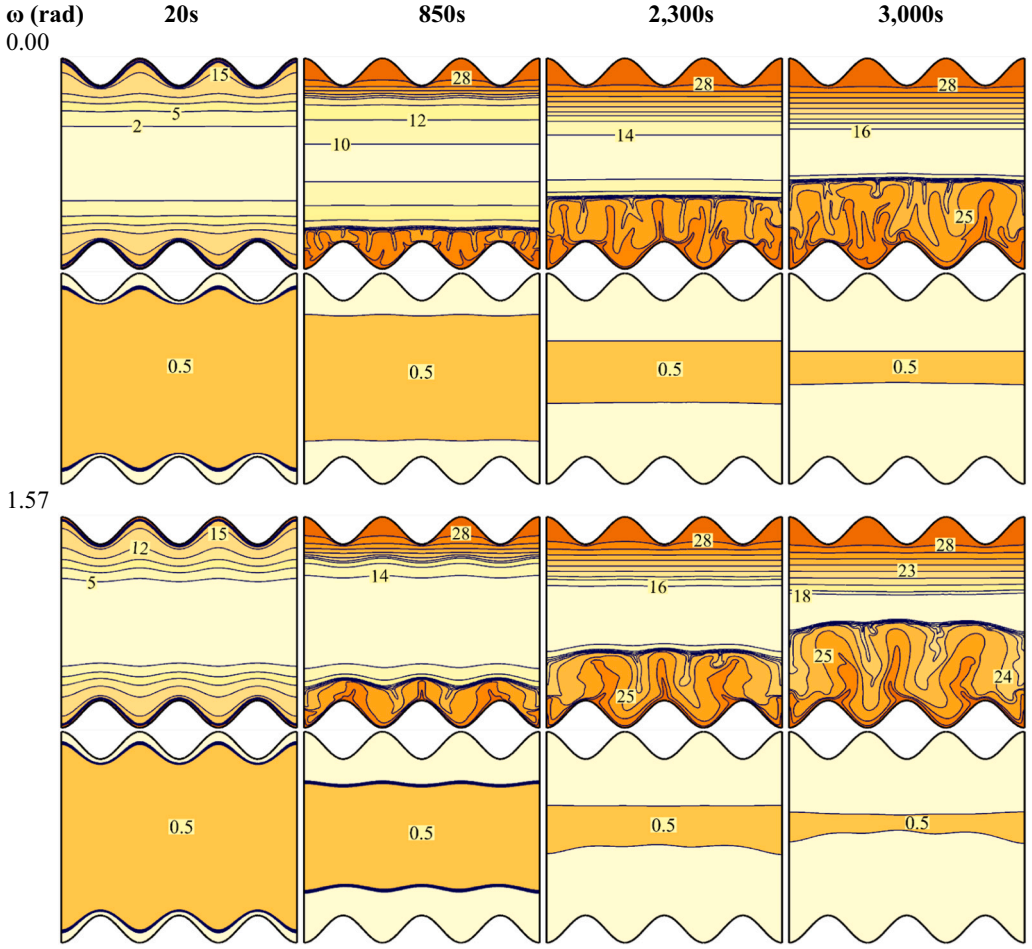

Fig. 8. Isotherms in the form of T-T_0 in °C (first row) and the melting interface (second row) at selected melting times for $\omega = 0$ rad and $\omega = 1.57$ rad.

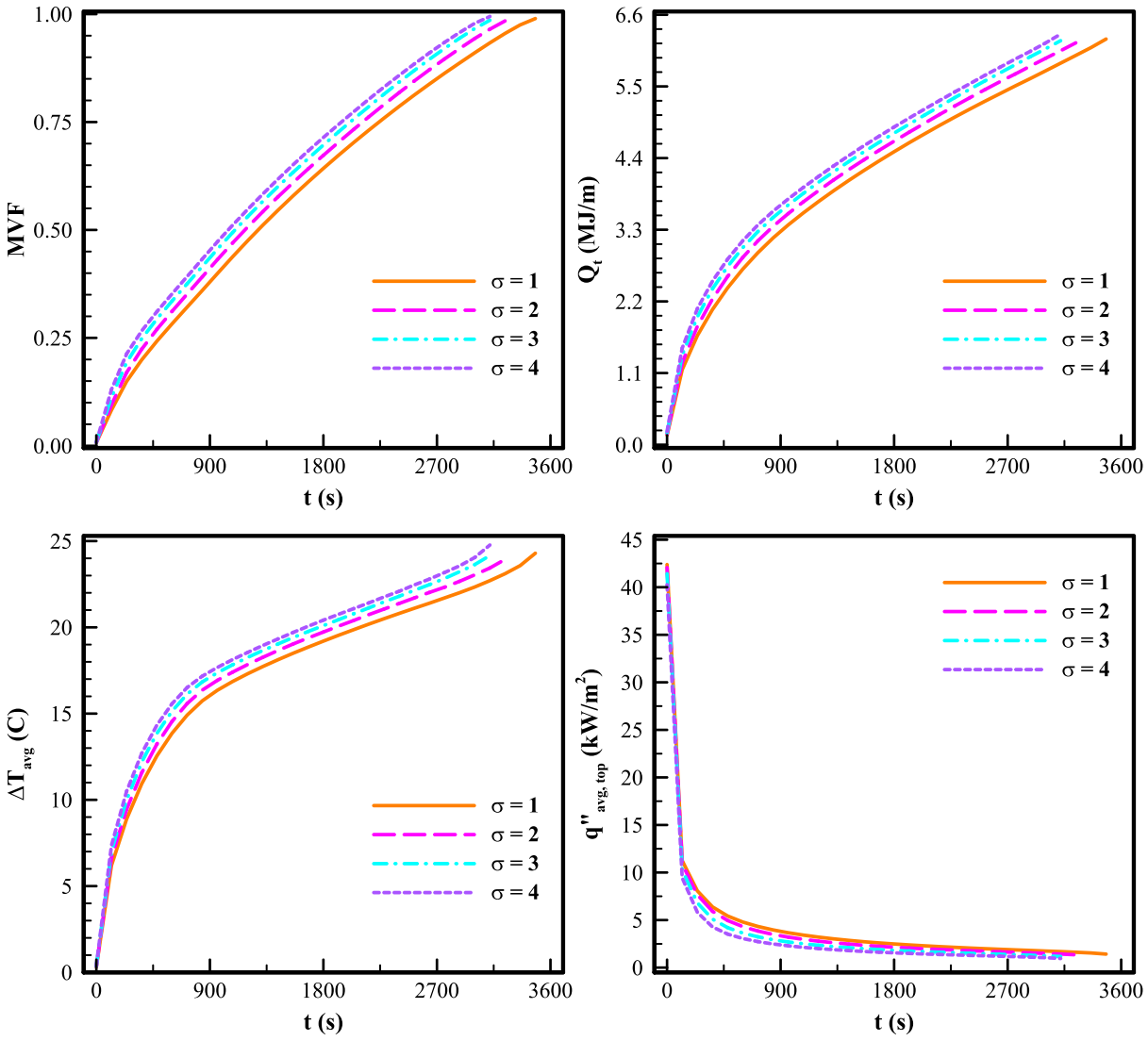

Fig. 9. MVF, total heat transfer (Q_t), average temperature difference (ΔT_{avg}), and the top wall Nusselt number over the melting time for different σ.

isotherm deflections in the lower region, suggesting robust convective circulation. Additionally, greater wave numbers lead to an expansion of the molten zones at both the top and bottom regions, signifying an improved melting process. The isotherm patterns in the upper region closely follow the contours of the heated wavy wall, reflecting the stratified nature of heat transfer in that specific zone.

5. Heat transfer analysis by using the neural networks

Calculating heat transfer during phase changes demands significant computational resources. As shown in Table 2, the selected mesh configuration with $Nm = 4$ takes approximately 733 min to compute. To better understand the impact of different design parameters on physical systems, neural networks (NNs) are utilized to examine the correlation between control variables and heat transfer rates. The network under consideration features three interconnected hidden layers, each comprising 20 neurons with sigmoid activation functions, as illustrated in Fig. 11. Experimenting with various network architectures determined the configuration of the neural network's layers and neurons. The final selected architecture, also shown in Fig. 11, has demonstrated effective training and testing performance.

Thus, the adopted neural network architecture resulted from methodical testing and evaluation aimed at achieving a balance between complexity and performance tailored to the specific characteristics of our dataset. This architecture demonstrated the best performance regarding learning ability and prediction accuracy for the range of parameters we investigated.

The training dataset includes 48 distinct cases, resulting in 5048 samples that cover a broad spectrum of parameters. These are elaborated on in the results section. Table 3 lists the input and output variables handled by the neural network and details the range of each input parameter.

Before initiating the training phase, the dataset underwent randomization, designating 70 % for training while equally partitioning the remaining 30 % for testing and validation. The primary objective during the training regimen was to curtail the Mean Squared Error (MSE) using the Adam optimizer [57]. With batch sizes of 4, the neural network underwent 1000 epochs. Data normalization was carried out using the StandardScaler technique [58]. The resulting training and validation loss metrics both reached an impressively low value of 8.05×10^{-4}.

Fig. 12 tracks the declining trend of MSE for both training and validation datasets over multiple epochs, indicating a consistent improvement. Fig. 13 contrasts the projected test data with the actual figures, corroborating the model's strong alignment with reality. Utilizing the high accuracy of this ANN, contour plots were generated to

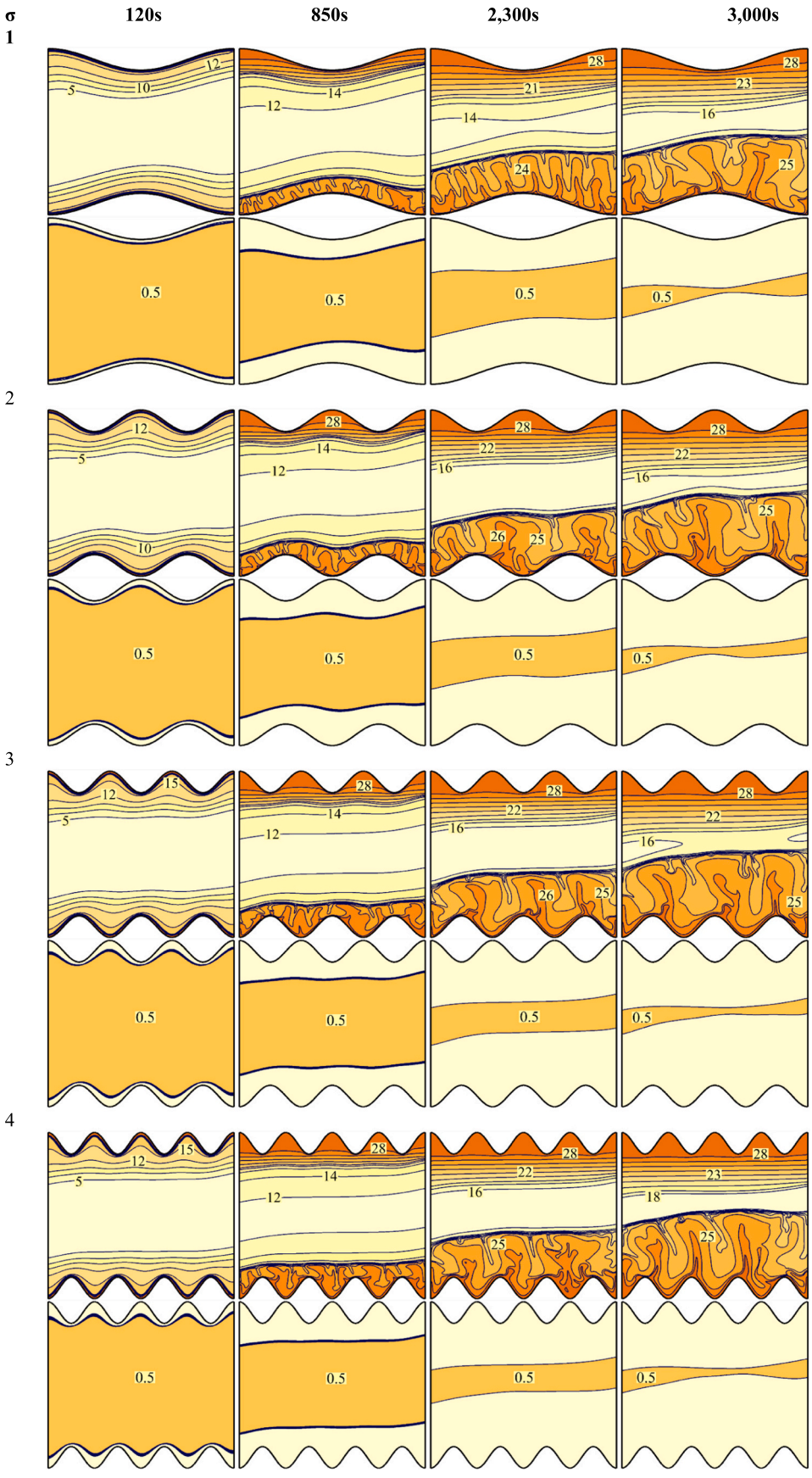

Fig. 10. Isotherms and MVF contours at selected melting times for different σ.

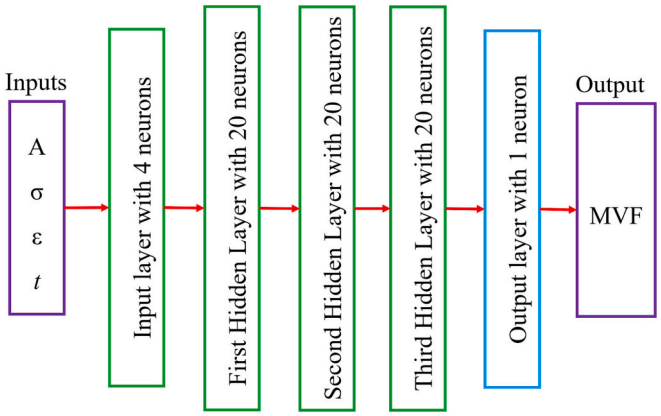

Fig. 11. A diagram of the employed neural network for learning the physical behavior of the LHTES unit.

Table 3
Inventory of neural network input and output variables.

Input parameters		Interval
Note	Symbol	
Porosity	ε	$0.9 < \varepsilon < 0.975$
Time (s)	t	$0 < t < 6840$
Wave amplitude (m)	A	$0.01125 < A < 0.0225$
Wave number	σ	$0 < \sigma < 4$

Output parameters		Interval
Note	Symbol	
Stored energy (MJ/m)	Q_t	$0 < Q_t < 6.7$
Melting volume fraction	MVF	$0 < MVF < 1$

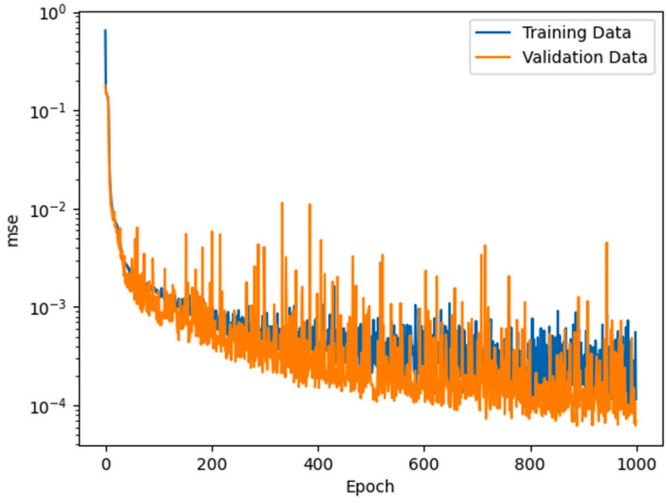

Fig. 12. Training and validation data over multiple epochs.

clarify the impact of various control parameters on the MVF.

Figs. 14 and 15 examine how porosity and wave amplitude influence MVF under two conditions: $\sigma = 2$ and $\sigma = 3$, respectively. For each scenario, snapshots are captured at two distinct times: $t = 1000$ (s) and $t = 1500$ (s). Fig. 14 reveals that as time elapses, the overall MVF tends to rise. Specifically, at $\sigma = 2$, MVF generally diminishes with increased porosity. On the flip side, keeping porosity constant while elevating wave amplitude leads to a higher MVF. Nevertheless, when porosity exceeds 92.5 ($\varepsilon > 92.5$), augmenting the wave amplitude beyond 0.025 (m) ceases to enhance MVF. In scenarios where $\varepsilon = 0.9$, elevating the wave amplitude to 0.03 (m) still yields benefits at $t = 1500$ (s).

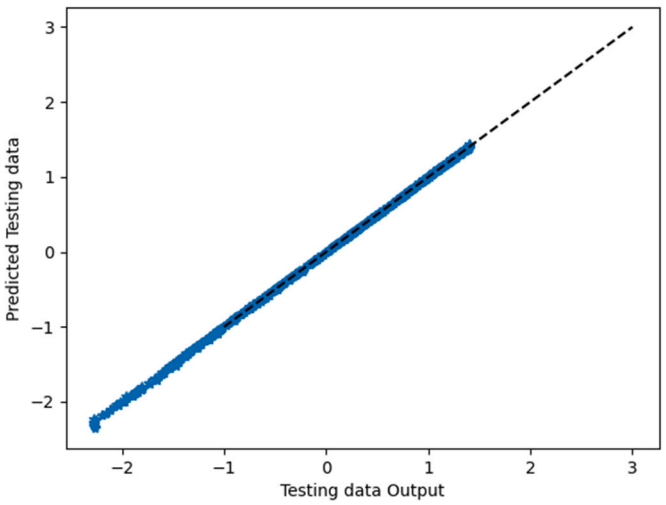

Fig. 13. Comparison between the actual and forecasted test data values.

Fig. 15 mirrors the trends observed in Fig. 14 when $t = 1000$ (s). However, as melting progresses to $t = 1500$ (s), elevating the wave amplitude seems to be consistently beneficial, irrespective of the porosity levels. Furthermore, a $\sigma = 3$ scenario (Fig. 15) consistently results in a higher MVF than its $\sigma = 2$ counterpart (Fig. 14).

These visualizations offer critical insights into the LHTES unit's responses to varying control parameters. They are the outcomes of extensive model simulations for numerous design configurations facilitated by the trained NNs. Performing direct simulations for such a multitude of design scenarios would demand several months of computational resources. Therefore, NNs serve as an invaluable asset for deeper analyses and simulations concerning LHTES design.

6. Conclusions

This study presented a comprehensive analysis of LHTES within a wavy enclosure filled with anisotropic copper metal foam saturated by paraffin wax. The top and bottom wavy walls of the enclosure are subjected to a high-temperature fluid stream, while the side walls are well-insulated. This configuration was modeled to examine the melting process of paraffin wax, which serves as the PCM. The model employed a set of control equations for the conservation of energy, mass, and momentum, solved through the FEM for both paraffin and metal foam.

One of the distinctive aspects of the study is the introduction of wavy wall topographies characterized by wave amplitude and wave number. The results are presented in the form of characteristic curves (key parameters) and contours. Augmenting the wave amplitude (A) from 3.75 mm to 18.75 mm diminishes the complete melting duration from 3600 s to 2700 s, resulting in a 25 % reduction in the melting time.

Additionally, this research incorporates NN models to scrutinize relationships between control variables and heat transfer rates. Utilizing a high-accuracy ANN model, contour plots are generated that offer critical insights into the system's response to varying parameters such as wave amplitude, wave number, and porosity. This methodology significantly reduces the computational time, enabling the analysis of extensive design configurations that would otherwise demand months of computational resources. The results showed that an increasing wave amplitude generally augments the MVF, stored thermal energy, and average temperature within the LHTES unit but slightly reduces the average heat flux at the top wavy wall.

The study also explores the effects of anisotropic angles in the metal foam, demonstrating that a 90° anisotropic angle significantly enhances all key performance indicators without adding any material or weight to

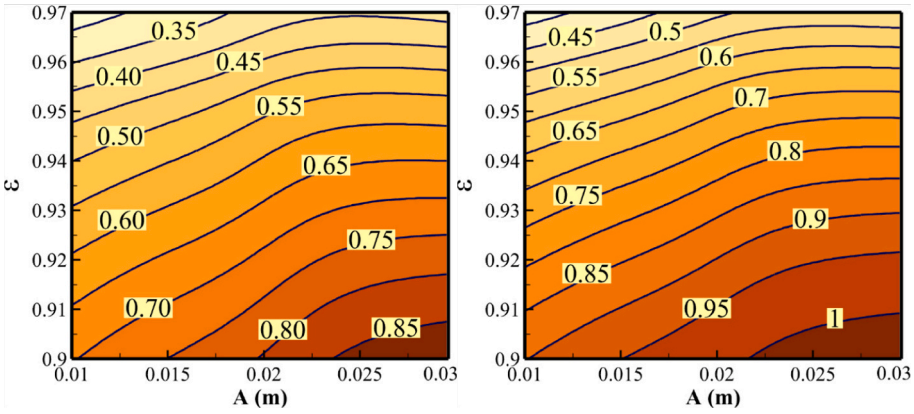

Fig. 14. The impact of porosity and wave amplitude on MVF for σ = 2 when (a) t = 1000 (s), and (b) t = 1500 (s).

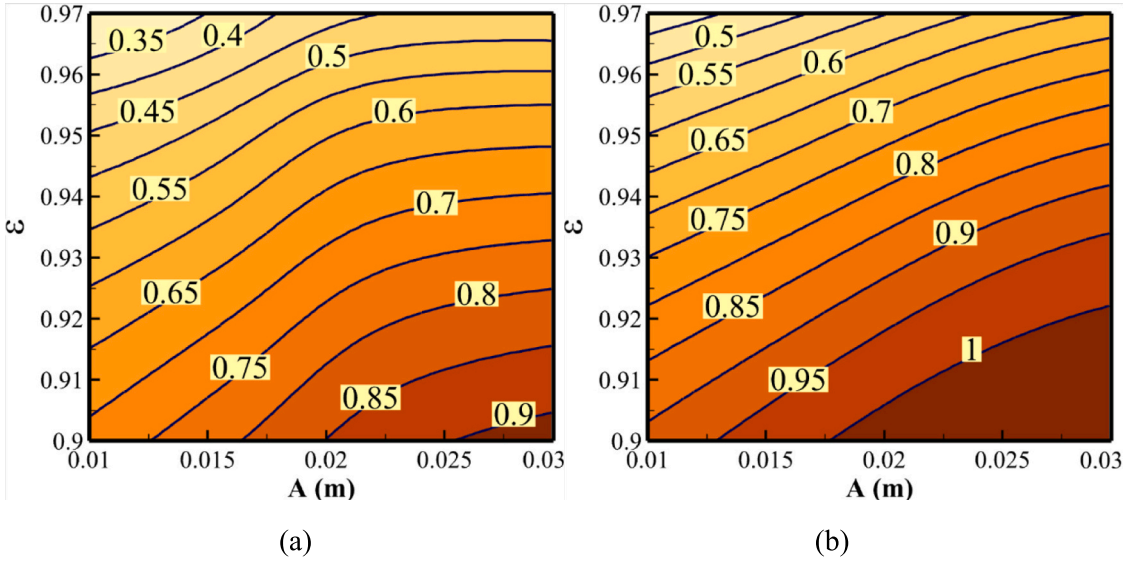

Fig. 15. The impact of porosity and wave amplitude on MVF for σ = 3 when (a) t = 1000 (s), and (b) t = 1500 (s).

the system. Elevating the anisotropic angle from 0° to 90° decreases the entire melting duration from 3750 s to 2500 s, culminating in a 33 % reduction in melting time. Thus, using a well-designed anisotropic MF can reduce the size and weight of LHTES units or increase their power rate.

Elevating the wave number beyond a certain limit (σ = 3 in this study) offers limited advantages in terms of MVF and stored thermal energy. NN stands out as an effective instrument for unraveling intricate relationships among diverse control parameters. This leads to a significant reduction in the computational time required to analyze extensive design scenarios.

The findings of this study highlight the notable effects of wavy wall configurations and anisotropic media on phase change heat transfer. Optimizing the anisotropic angle can decrease melting time by 33 % without the need for additional weight or materials. By tailoring the directional properties of metal foam, energy storage duration can be reduced by 33 %. Additionally, incorporating a wavy structure can lead to a 25 % reduction in melting time. These enhancements are particularly beneficial for domestic solar energy storage systems, enabling faster storage of surplus heat. Moreover, such significant decreases in melting time are also valuable in managing the temperature of vehicle batteries, where weight is a crucial consideration. Therefore, future research should explore the impact of anisotropic metal foams and wavy structures on the thermal management of vehicle batteries.

CRediT authorship contribution statement

Hakim S. Sultan: Conceptualization, Data curation, Formal analysis, Methodology, Supervision, Writing – original draft. **Mohammed Hasan Ali:** Data curation, Formal analysis, Investigation, Writing – original draft, Writing – review & editing. **Jana Shafi:** Data curation, Formal analysis, Investigation, Software, Visualization, Writing – original draft, Writing – review & editing. **Mehdi Fteiti:** Formal analysis, Investigation, Methodology, Writing – original draft, Writing – review & editing. **Manuel Baro:** Formal analysis, Investigation, Methodology, Writing – review & editing. **Khalid Almutairi:** Formal analysis, Investigation, Methodology, Supervision, Writing – original draft, Writing – review & editing. **Mohammad S. Islam:** Investigation, Methodology, Writing – original draft. **Kamal Harb:** Formal analysis, Investigation, Writing – review & editing. **Fawaz S. Alharbi:** Investigation, Methodology, Writing – review & editing. **Mohammad Ghalambaz:** Conceptualization, Software, Supervision, Validation, Visualization.

Declaration of competing interest

The authors clarify that there is no conflict of interest for report.

Data availability

No data was used for the research described in the article.

Acknowledgments

The authors would like to thank the Deanship of Scientific Research at Umm Al-Qura University for supporting this work by Grant Code: (23UQU4310414DSR08). This research of Mohammad Ghalambaz was supported by the Tomsk State University Development Programme (Priority-2030).

References

[1] J. Paul, A. Pandey, Y.N. Mishra, Z. Said, Y.K. Mishra, Z. Ma, J. Jacob, K. Kadirgama, M. Samykano, V. Tyagi, Nano-enhanced organic form stable PCMs for medium temperature solar thermal energy harvesting: recent progresses, challenges, and opportunities, Renew. Sustain. Energy Rev. 161 (2022), 112321.
[2] K. Du, J. Calautit, P. Eames, Y. Wu, A state-of-the-art review of the application of phase change materials (PCM) in Mobilized-Thermal Energy Storage (M-TES) for recovering low-temperature industrial waste heat (IWH) for distributed heat supply, Renew. Energy 168 (2021) 1040–1057.
[3] S. Wu, T. Yan, Z. Kuai, W. Pan, Thermal conductivity enhancement on phase change materials for thermal energy storage: a review, Energy Storage Materials 25 (2020) 251–295.
[4] T. Ma, Z. Guo, M. Lin, Q. Wang, Recent trends on nanofluid heat transfer machine learning research applied to renewable energy, Renew. Sustain. Energy Rev. 138 (2021), 110494.
[5] D.R.E. Ewim, M.O. Okwu, E.J. Onyiriuka, A.S. Abiodun, S.M. Abolarin, A. Kaood, A Quick Review of the Applications of Artificial Neural Networks (ANN) in the Modelling of Thermal Systems, 2021.
[6] A. Alsabery, H. Kadhim, M. Ismael, I. Hashim, A. Chamkha, Impacts of amplitude and heat source on natural convection of hybrid nanofluids into a wavy enclosure via heatline approach, Waves Random Complex Media 33 (4) (2023) 1060–1084.
[7] F.M. Azizul, A.I. Alsabery, I. Hashim, R. Roslan, H. Saleh, MHD mixed convection and heatlines approach of nanofluids in rectangular wavy enclosures with multiple solid fins, Sci. Rep. 13 (1) (2023) 9660.
[8] A.I. Alsabery, M.H. Yazdi, E. Solomin, H.F. Öztop, I. Hashim, Evaluation of convection flow and entropy generation in a wavy cubical container with nanofluid and embedded cylinder, Journal of Computational Design and Engineering 9 (2) (2022) 598–615.
[9] F.J. Gumir, K. Al-Farhany, W. Jamshed, E.S.M. Tag El Din, A. Abd-Elmonem, Natural convection in a porous cavity filled (35% MWCNT-65% Fe3O4)/water hybrid nanofluid with a solid wavy wall via Galerkin finite-element process, Sci. Rep. 12 (1) (2022) 17794.
[10] P. Barman, P. Rao, Effect of aspect ratio on natural convection in a wavy porous cavity submitted to a partial heat source, International Communications in Heat and Mass Transfer 126 (2021), 105453.
[11] H.T. Kadhim, F.A. Jabbar, A. Rona, Cu-Al2O3 hybrid nanofluid natural convection in an inclined enclosure with wavy walls partially layered by porous medium, Int. J. Mech. Sci. 186 (2020), 105889.
[12] A.I. Alsabery, M.H. Yazdi, A.S. Abosinnee, I. Hashim, E. Solomin, Impact of partial slip condition on mixed convection of nanofluid within lid-driven wavy cavity and solid inner body, Propulsion and Power Research 11 (4) (2022) 544–564.
[13] I.A. Laasri, Z. Elmaazouzi, A. Outzourhit, M.O. Mghazli, Investigation of different topology-optimized fin structures in a cylindrical latent heat thermal energy storage unit, Thermal Science and Engineering Progress 33 (2022), 101372.
[14] A. Tavakoli, J. Hashemi, M. Najafian, A. Ebrahimi, Physics-based modelling and data-driven optimisation of a latent heat thermal energy storage system with corrugated fins, Renew. Energy 217 (2023), 119200.
[15] J. Wu, N. Li, Z. Wu, Experimental investigation of latent energy storage systems with the tree-pin-shaped fin, Appl. Therm. Eng. 227 (2023), 120370.
[16] N.S. Bondareva, M.A. Sheremet, Influence of metal foam and nanoparticles on convective melting in a rectangular cavity under heating of bottom wall, International Journal of Thermofluids 19 (2023), 100374.
[17] Z. Haddad, F. Iachachene, M.A. Sheremet, E. Abu-Nada, Numerical investigation and optimization of melting performance for thermal energy storage system partially filled with metal foam layer: new design configurations, Appl. Therm. Eng. 223 (2023), 119809.
[18] S. Sabet, B. Buonomo, M.A. Sheremet, O. Manca, Numerical investigation of melting process for phase change material (PCM) embedded in metal foam structures with Kelvin cells at pore scale level, International Journal of Heat and Mass Transfer 214 (2023), 124440.
[19] M. Fteiti, M. Ghalambaz, M. Sheremet, M. Ghalambaz, The impact of random porosity distribution on the composite metal foam-phase change heat transfer for thermal energy storage, Journal of Energy Storage 60 (2023), 106586.
[20] M. Ghalambaz, M. Aljaghtham, A.J. Chamkha, A. Abdullah, A. Alshehri, M. Ghalambaz, Anisotropic metal foam design for improved latent heat thermal energy storage in a tilted enclosure, International Journal of Mechanical Sciences 238 (2023), 107830.
[21] J.M. Mahdi, H.I. Mohammed, P. Talebizadehsardari, M. Ghalambaz, H.S. Majdi, W. Yaïci, D. Giddings, Simultaneous and consecutive charging and discharging of a PCM-based domestic air heater with metal foam, Appl. Therm. Eng. 197 (2021), 117408.
[22] M. Ghalambaz, J. Zhang, Conjugate solid-liquid phase change heat transfer in heatsink filled with phase change material-metal foam, International Journal of Heat and Mass Transfer 146 (2020), 118832.
[23] M. Ghalambaz, A.A. Melaibari, A.J. Chamkha, O. Younis, M. Sheremet, Phase change heat transfer and energy storage in a wavy-tube thermal storage unit filled with a nano-enhanced phase change material and metal foams, Journal of Energy Storage 54 (2022), 105277.
[24] F. Iachachene, Z. Haddad, H.F. Oztop, E. Abu-Nada, Melting of phase change materials in a trapezoidal cavity: orientation and nanoparticles effects, J. Mol. Liq. 292 (2019), 110592.
[25] F. Ahmad, S. Hussain, I. Ahmad, T.S. Hassan, A.O. Almatroud, W. Ali, I.E. Farooq, Successive melting of a phase change material bounded in a finned trapezoidal domain, Case Studies in Thermal Engineering 28 (2021), 101419.
[26] M.A. Fteiti, M. Ghalambaz, O. Younis, M. Sheremet, M. Ismael, The influence of the metal foam layer shape on the thermal charging response time of a latent heat thermal energy storage system, Journal of Energy Storage 58 (2023), 106284.
[27] P.C. Singh, P. Halder, Performance assessment of an air-conditioning system utilizing a PCM-based annulus cylindrical latent heat storage, Arab. J. Sci. Eng. (2023) 1–12.
[28] S. Motahar, M. Jahangiri, Transient heat transfer analysis of a phase change material heat sink using experimental data and artificial neural network, Appl. Therm. Eng. 167 (2020), 114817.
[29] M. Sheikholeslami, M.B. Gerdroodbary, R. Moradi, A. Shafee, Z. Li, Application of Neural Network for estimation of heat transfer treatment of Al2O3-H2O nanofluid through a channel, Comput. Methods Appl. Mech. Eng. 344 (2019) 1–12.
[30] A. Maleki, M. Elahi, M.E.H. Assad, M. Alhuyi Nazari, M. Safdari Shadloo, N. Nabipour, Thermal conductivity modeling of nanofluids with ZnO particles by using approaches based on artificial neural network and MARS, Journal of Thermal Analysis and Calorimetry 143 (2021) 4261–4272.
[31] A. Komeilibirjandi, A.H. Raffiee, A. Maleki, M. Alhuyi Nazari, M. Safdari Shadloo, Thermal conductivity prediction of nanofluids containing CuO nanoparticles by using correlation and artificial neural network, J. Therm. Anal. Calorim. 139 (2020) 2679–2689.
[32] A.I.N. Korti, H. Guellil, Experimental study of the effect of inclination angle on the paraffin melting process in a square cavity, Journal of Energy Storage 32 (2020), 101726.
[33] M. Iasiello, N. Bianco, W.K. Chiu, V. Naso, Anisotropic convective heat transfer in open-cell metal foams: assessment and correlations, International Journal of Heat and Mass Transfer 154 (2020), 119682.
[34] M. Ghalambaz, M. Aljaghtham, A.J. Chamkha, A. Abdullah, I. Mansir, M. Ghalambaz, Mathematical modeling of heterogeneous metal foams for phase-change heat transfer enhancement of latent heat thermal energy storage units, App. Math. Model. 115 (2023) 398–413.
[35] S. Zhang, Y. Yao, Y. Jin, Z. Shang, Y. Yan, Heat transfer characteristics of ceramic foam/molten salt composite phase change material (CPCM) for medium-temperature thermal energy storage, International Journal of Heat and Mass Transfer 196 (2022), 123262.
[36] D.A. Nield, A. Bejan, Convection in Porous Media, Springer, 2006.
[37] Y. Yao, H. Wu, Z. Liu, Direct simulation of interstitial heat transfer coefficient between paraffin and high porosity open-cell metal foam, J. Heat Transfer 140 (3) (2018).
[38] A. Ebrahimi, C.R. Kleijn, I.M. Richardson, Sensitivity of numerical predictions to the permeability coefficient in simulations of melting and solidification using the enthalpy-porosity method, Energies 12 (22) (2019) 4360.
[39] M. Hameter, H. Walter, Influence of the mushy zone constant on the numerical simulation of the melting and solidification process of phase change materials, in: Computer Aided Chemical Engineering, Elsevier, 2016, pp. 439–444.
[40] A.S. Soliman, A.A. Sultan, M.A. Sultan, Effect of mushy zone parameter on phase change behavior of different configurations storage unit: numerical simulation and experimental validation, Sustainability 14 (21) (2022) 14540.
[41] Y. Yao, H. Wu, Interfacial heat transfer in metal foam porous media (MFPM) under steady thermal conduction condition and extension of Lemlich foam conductivity theory, International Journal of Heat and Mass Transfer 169 (2021), 120974.
[42] C. Zhao, J. Wang, Y. Sun, S. He, K. Hooman, Fin design optimization to enhance PCM melting rate inside a rectangular enclosure, Appl. Energy 321 (2022), 119368.
[43] M. Ghalambaz, M. Aljaghtham, A.J. Chamkha, A. Abdullah, A. Alshehri, M. Ghalambaz, An anisotropic metal foam design for improved latent heat thermal energy storage in a tilted enclosure, International Journal of Mechanical Sciences 238 (2022), 107830.
[44] Y. Yao, H. Wu, Macroscale modeling of solid–liquid phase change in metal foam/paraffin composite: effects of paraffin density treatment, thermal dispersion, and interstitial heat transfer, Journal of Thermal Science and Engineering Applications 13 (4) (2021).
[45] A. Agarwal, R. Sarviya, Characterization of commercial grade paraffin wax as latent heat storage material for solar dryers, Materials Today: Proceedings 4 (2) (2017) 779–789.

[46] N. Ukrainczyk, S. Kurajica, J. Šipušić, Thermophysical comparison of five commercial paraffin waxes as latent heat storage materials, Chem. Biochem. Eng. Q. 24 (2) (2010) 129–137.
[47] H. Zheng, C. Wang, Q. Liu, Z. Tian, X. Fan, Thermal performance of copper foam/paraffin composite phase change material, Energy Convers. Manag. 157 (2018) 372–381.
[48] A.I.N. Korti, H. Guellil, Experimental study of the effect of inclination angle on the paraffin melting process in a square cavity, J. Energy Storage 32 (2020), 101726.
[49] A. Agarwal, R. Sarviya, Characterization of commercial grade paraffin wax as latent heat storage material for solar dryers, Mater. Today: Proc. 4 (2) (2017) 779–789.
[50] N. Ukrainczyk, S. Kurajica, J. Šipušić, Thermophysical comparison of five commercial paraffin waxes as latent heat storage materials, Chem. Biochem. Eng. Q. 24 (2) (2010) 129–137.
[51] C.T. Kelley, Solving Nonlinear Equations With Newton's Method, SIAM, 2003.
[52] P. Deuflhard, Newton Methods for Nonlinear Problems: Affine Invariance and Adaptive Algorithms, Springer Science & Business Media, 2005.
[53] O.C. Zienkiewicz, R.L. Taylor, P. Nithiarasu, The Finite Element Method for Fluid Dynamics, Seventh ed., Butterworth-Heinemann, Oxford, 2014.
[54] D. Pepper, The Intermediate Finite Element Method: Fluid Flow and Heat Transfer Applications, Routledge, 2017.
[55] B. Kamkari, H.J. Amlashi, Numerical simulation and experimental verification of constrained melting of phase change material in inclined rectangular enclosures, International Communications in Heat and Mass Transfer 88 (2017) 211–219.
[56] B. Kamkari, H. Shokouhmand, F. Bruno, Experimental investigation of the effect of inclination angle on convection-driven melting of phase change material in a rectangular enclosure, Int. J. Heat Mass Transf. 72 (2014) 186–200.
[57] I.K.M. Jais, A.R. Ismail, S.Q. Nisa, Adam optimization algorithm for wide and deep neural network, Knowledge Engineering and Data Science 2 (1) (2019) 41–46.
[58] Scikit-Learn, sklearn.preprocessing.StandardScaler, Scikit-Learn, 2023.